JOTCS A
Journal of the Turkish Chemical Society
Section: A
Chemistry
TURKISH CHEMICAL SOCIETY

Biosorption of Methyl Orange Dye in Single, Binary and Ternary System onto Gingerbread Plum Seed Shell Activated Carbon

Musa Husaini[1*], Bishir Usman[1], Muhammad Bashir Ibrahim[1]

[1]Department of Pure and Industrial Chemistry, Faculty of Physical Sciences College of Natural and Pharmaceutical Sciences, Bayero University Kano (BUK), P.M.B. 3011, Kano, Nigeria.

Abstract: The research investigated the potential of gingerbread plum seed shell activated to function as a biosorbent for eliminating methyl orange (MO) dye from water in various dye combinations, including single, binary, and ternary systems alongside methylene blue (MB) and Congo red (CR) dyes. The characteristics of the adsorbent were analyzed through techniques like Scanning Electron Microscopy, Fourier Transform Infrared spectroscopy, and pH point of zero charges. Batch adsorption tests were conducted to examine the adsorption processes' equilibrium behaviors, thermodynamics, and kinetics. The collected data were subjected to different isotherm and kinetics equations. The pseudo-second-order kinetics model provided the best fit for all the sorption systems, irrespective of composition differences, with higher rate constants observed for binary MO+MB= 0.031 g/mg/min system and lower for binary MO+CR= 0.028 g/mg/min and ternary MO+MB+CR= 0.029 g/mg/min systems compared to the single system MO= 0.030 g/mg/min. The maximum monolayer capacity of the adsorbent for methyl orange demonstrated synergistic interaction with the presence of methylene blue and antagonistic interaction with the presence of Congo red dye. The findings indicated that the adsorption processes varied based on the system's composition; they were all spontaneous (with ΔG values ranging from -1.146 to -10.415 kJ/mol) and exothermic (with ΔH values between -17.94 and -54.63 kJ/mol). Additionally, randomness decreased, as reflected by ΔS values of -054.43 and -382.62 J/K for the entire process.

Keywords: Adsorption, Equilibrium study, Kinetic study, Thermodynamic study, Synergistic effect, and antagonistic effect.

Submitted: October 8, 2023. **Accepted:** February 5, 2024.

Cite this: Husaini M, Usman B, Ibrahim MB. Biosorption of Methyl Orange Dye in Single, Binary and Ternary System onto Gingerbread Plum Seed Shell Activated Carbon. JOTCSA. 2024;11(2):655-64.

DOI: https://doi.org/10.18596/jotcsa.1372995

***Corresponding author's E-mail:** musahusaini36@gmail.com

1. INTRODUCTION

Dye contaminants in wastewater are a notable environmental hazard due to their enduring and detrimental characteristics, posing risks to human health and marine ecosystems (1). The discharge of dye-containing wastewater, even in minimal concentrations, is aesthetically displeasing and environmentally troublesome, especially when originating from textile industries. Therefore, effectively removing dyes from such wastewater is essential to address ecological, biological, and industrial challenges (2). Numerous approaches have been developed to address this issue, such as chemical ion exchange, membrane filtration, physical adsorption, photocatalysis, and biological methods.

Adsorption stands out among these methods as a promising approach thanks to its simplicity, high effectiveness, and cost-efficiency (3). The choice of adsorbent significantly impacts the effectiveness of adsorption processes. Cost-effective adsorbents that possess a high adsorption capacity and can be easily reused are preferred (4).

Due to its favorable characteristics like high yield during production, cost-effectiveness, eco-friendliness, and effective adsorption capabilities, activated carbon derived from carbon-rich organic materials has been extensively studied for removing pollutants from wastewater (5,6). Activated carbon from various waste sources, such as sugarcane bagasse and peanut biomass, have been investigated for their potential in dye removal from water (7,8). However, industrial wastewater typically contains multiple dyes concurrently. The adsorption behavior of one dye may change when other dyes are present (9). While there is a substantial body of research on

adsorption involving single components (10,11) or binary combinations (12,13), knowledge regarding the removal of dyes in complex mixtures is more limited (14,15).

The lack of research in this area adds complexity to understanding the adsorption process for industrial wastewater with multiple components. While some agricultural waste materials have been tested for the removal of a single dye, very few have been explored for the removal of multiple dyes. This study specifically focuses on utilizing activated carbon derived from gingerbread plum seed shells to adsorb Congo red in a competitive environment. The potential of this agricultural waste in removing the dye in a competitive setting has not been investigated previously.

2. METHODOLOGY

2.1 Activated Carbon Preparation

The adsorbent sample was prepared following the method outlined in references (16,17). Gingerbread plum seed shell samples were collected and cleaned with tap water to remove impurities. Afterward, they were allowed to naturally air-dry for 72 hours. The dried samples were then finely ground to achieve a granular texture and immersed in a solution containing 30% phosphoric acid (CAS 7663-38-2) for 24 hours. After impregnation, the samples were dried and subjected to carbonization in a furnace at a temperature of 400 °C for 2 hours. The resulting activated samples underwent a thorough rinsing process using distilled water until a neutral solution was attained. They were then dried in an oven at 105 °C until a consistent weight was reached. Subsequently, the samples were sieved and stored in an airtight container (17,18).

2.2 Adsorbent Characterization

To analyze the characteristics of activated carbon derived from gingerbread plum seed shells, its infrared spectra were recorded before and after dye absorption using an FTIR spectrophotometer spanning from 4000 cm^{-1} to 600 cm^{-1}. The surface morphology of the adsorbent was assessed through scanning electron microscopy (19,20). The adsorbent's point of zero charge (pH_{zpc}) was determined following the procedure outlined (8). This involved adding 0.1 g of the adsorbent to a 40 mL solution of 0.1 M $NaNO_3$ (CAS 7631-99-4) with a predefined initial pH (pH_i). In separate adsorbent flasks, initial pH levels were adjusted using 0.1 M NaOH (CAS 1310-73-2) or HCl (CAS 7647-01-0). After agitating the flasks for 24 hours, the final pH (pH_f) was measured using a pH meter. Plotting the change in pH ($pH_i - pH_f$) against the initial pH yields the pH_{zpc}, where the plot intersects the horizontal axis (21).

2.3 Preparing the Adsorbate

The main substance under adsorption investigation is an anionic dye named Methyl Orange (MO) (CAS 547-58-0), provided by Sigma Aldrich. Different aqueous solutions of MO dye were made using varying concentrations from the dye's original solution (1000 mg/L) in the case of the single dye system. In the binary system, either Methylene Blue (MB) (CAS 61-73-4) dye or Congo Red (CR) (CAS 573-58-0) dye was mixed with predefined concentrations of the primary adsorbate. All three dyes were mixed in the ternary system. Figure 1 displays the chemical structure of these three dyes.

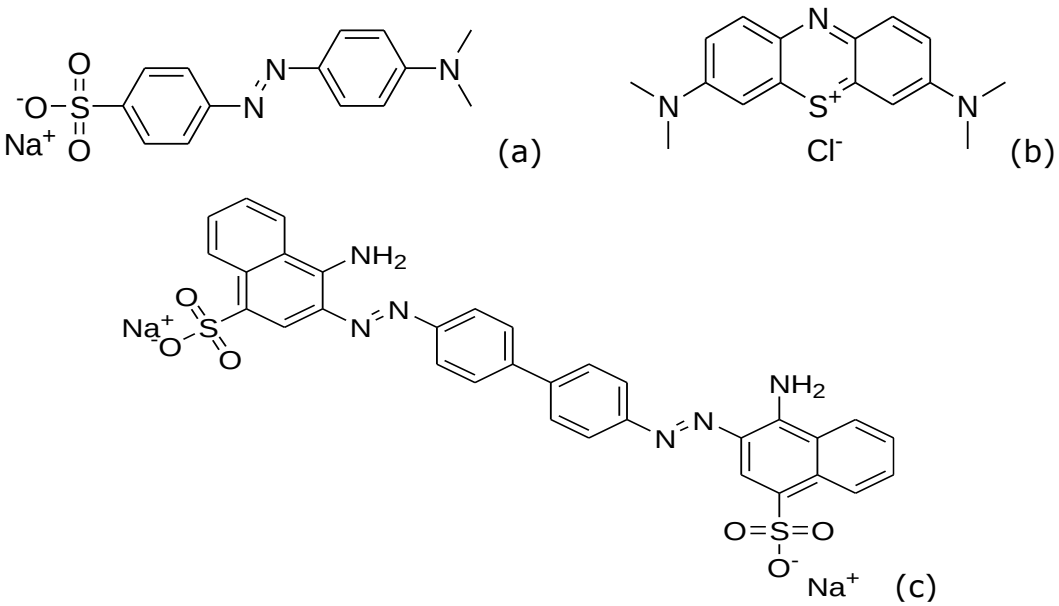

Figure 1: Structure of the Dyes (a) Methyl orange b) Methylene blue c) Congo red.

2.4 Batch Adsorption Experiment

Various solutions of methyl orange dye with differing concentrations and volume (50 mL each) were introduced into clearly labeled glass bottles containing a fixed amount of the adsorbent. These bottles were sealed with lids and placed in a thermostat-controlled horizontal mechanical shaker that maintained a consistent speed, temperature, and pH until equilibrium. Further rounds of batch experiments were conducted to explore the effects of adsorbent quantity (0.1 – 0.6 g), contact time (5 – 150 min), pH (2 – 12), and temperature (303 – 323

K). This involved using varying amounts of adsorbent, pre-determined contact durations, pH levels, and specific temperatures. Subsequently, the mixtures of dye and adsorbent in the flasks were filtered, and the absorbance of the filtrate was measured using a UV-visible scanning spectrophotometer at the specified absorption wavelength, λ_{max} (464.5 nm) of methyl orange dye (22).

The quantity of dye adsorbed per unit mass of adsorbent, denoted as q (mg/g), was calculated using formulas 1 and 2.

$$qe = \frac{(C_0 - C_e) \times v}{m} \quad (1)$$

$$qt = \frac{(C_0 - C_t) \times v}{m} \quad (2)$$

In this context, q_e and q_t denote the quantity of dye adsorbed (in mg/g) at equilibrium and at a specific time t, respectively. C_o, C_e, and C_t (measured in mg/L) represent the initial dye concentration (at t=0), dye concentration at equilibrium, and dye concentration at a given time t=t, respectively. V refers to the volume of the solution (in liters), while m indicates the mass of the adsorbent (in grams).

3. RESULTS AND DISCUSSION

3.1 Characterization

Figure 2 depicts the FTIR spectra of the adsorbent both before and after the adsorption of dye. The FTIR spectrum of activated carbon from gingerbread plum seed shell is composite, featuring multiple absorption peaks even prior to dye adsorption. Reflective of different functional groups, which are potential sites for adsorption of adsorbate (9). Following the adsorption of methyl orange, shifts in band positions of frequencies were evident in the FTIR spectrum of the adsorbent after adsorption (Table 1). These shifts in adsorption bands imply potential interaction between the surface of adsorbent and dye molecules.

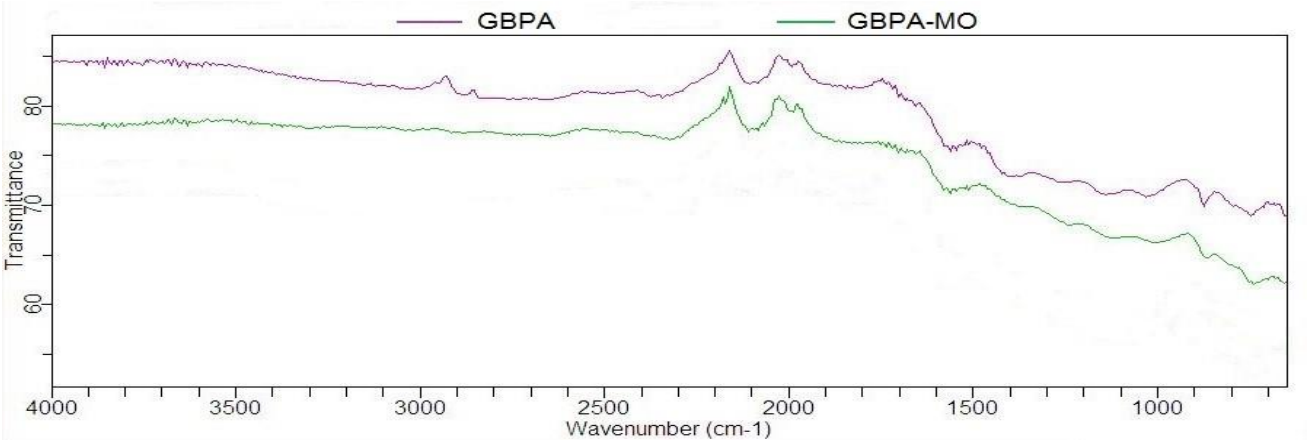

Figure 2: FTIR Analysis before (GBPA) and after Adsorption of MO (GBPA-MO).

Table 1: Functional group observed before and after adsorption of Methyl orange.

Functional group	Vibration Frequency (cm^{-1})	Observed Frequency (cm^{-1})	
		Before Adsorption	After Adsorption
O-H stretching vibration in alcohol	3700-3584	3661	3674
C-H stretching vibration in alkane	3000-2840	2880	2850
C ≡ C stretching vibration in alkyne	2260-2100	2191	2258
C ≡ C stretching vibration in alkyne	2260-2100	2107	2173
C=C=C stretching of allene	2000-1900	1994	1990
N-O stretching of nitro groups	1550-1500	1547	1562
C-O stretching of aliphatic ether	1150-1085	1140	1165
C-H bending of 1,3-disubstituted	880±20	870	866
C-H bending of monosubstituted	750±20	755	749

Additional characterization results are presented in Figure 3. The scanning electron micrograph of the adsorbent at ×1000 magnification (Figure 3a) displays an irregular and porous surface texture. This characteristic surface structure could signify a favorable attribute for an effective adsorbent with a substantial surface area. This surface was smoothed by the presence of dye molecules after the adsorption process (Figure 3b) (16,23).

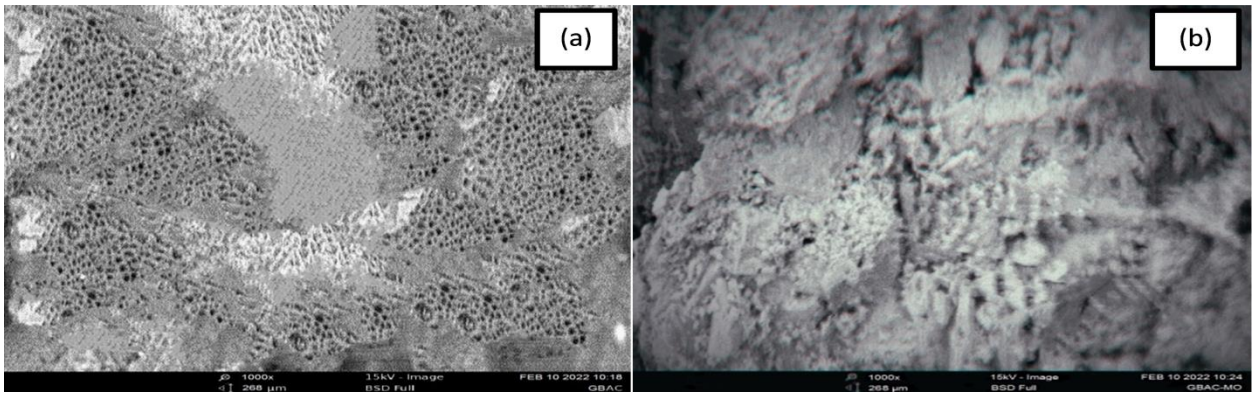

Figure 3: SEM Micrograph (a) before and (b) Adsorption of Methyl orange.

In Figure 4, the point of zero charge (pH_{zpc}) is depicted and found to be 5.60. Below this pH, the surface of the adsorbent carries a positive charge, which attracts negatively charged species in the solution. Conversely, above the p_{Hzpc}, the surface carries a negative charge, thereby attracting cations (24,25).

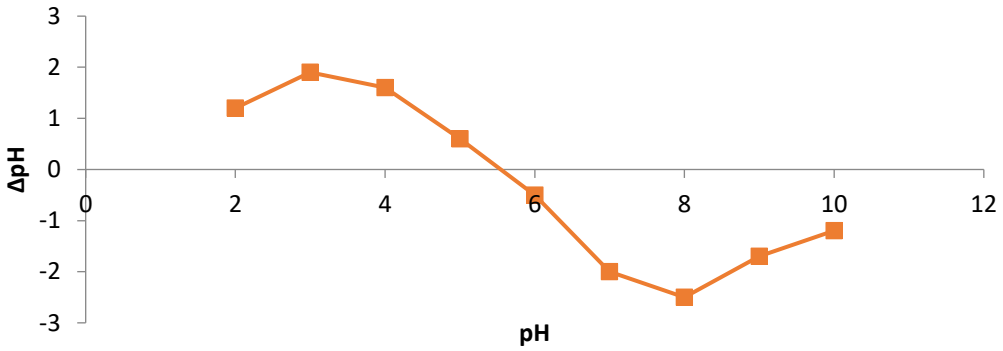

Figure 4: pH at point of zero charge of the adsorbent.

3.2 Influence of Solution pH

The pH level of an aqueous system plays a pivotal role in determining the chemical state and degree of ionization of the adsorbate during the adsorption process. This renders it a critical factor in wastewater treatment via adsorption. Figure 5 illustrates the influence of pH on the adsorption of methyl orange onto the adsorbent. The adsorption capacity (q_e) demonstrated a pronounced increase under acidic pH conditions, gradually diminishing as the pH level rose. This trend may be attributed to the heightened presence of OH^- ions, which compete with the anion groups on the dye for available adsorption sites on the adsorbent, especially with increasing pH. Moreover, when the pH is below the adsorbent's point of zero charge (pH_{zpc}), the adsorbent's surface holds a positive charge, facilitating the attraction of anionic dyes through electrostatic forces. This phenomenon amplifies the adsorption of methyl orange. (26,27) have also reported similar findings concerning the increased adsorption capacity of acid dyes in acidic pH conditions.

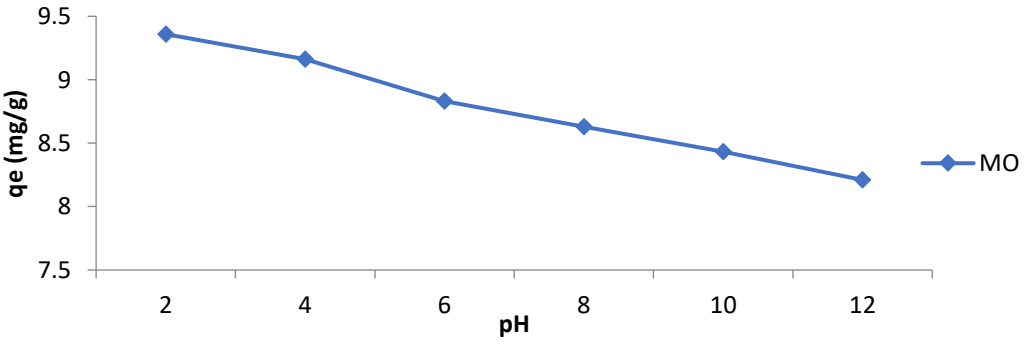

Figure 5: Effect of pH on adsorption of methyl orange.

3.3 Impact of Adsorbent Dosage

The quantity of methyl orange adsorbed per unit mass of adsorbent, indicated as qe, decreased as the

adsorbent dosage increased across various adsorbate systems (single, binary, and ternary), as shown in Figure 6a. With an increase in the adsorbent dose from 0.1 to 0.6 g, the adsorption capacity (q_e) consistently decreased from 9.70 to 8.99 mg/g in the single dye system containing only methyl orange, from 9.388 to 9.95 mg/g in the binary system with methyl orange and methylene blue (MO + MB), and from 8.30 to 7.599 mg/g in the binary system with methyl orange and Congo red (MO + CR). A reduction in the adsorption density (from 8.801 to 8.09 mg/g) was also observed in the ternary system containing all three dyes. These findings suggest that at lower doses, the active sites on the surface of the adsorbent were effectively utilized, but with an increase in the adsorbent dose, a significant portion of these active sites likely overlapped, resulting in a decrease in the specific uptake.

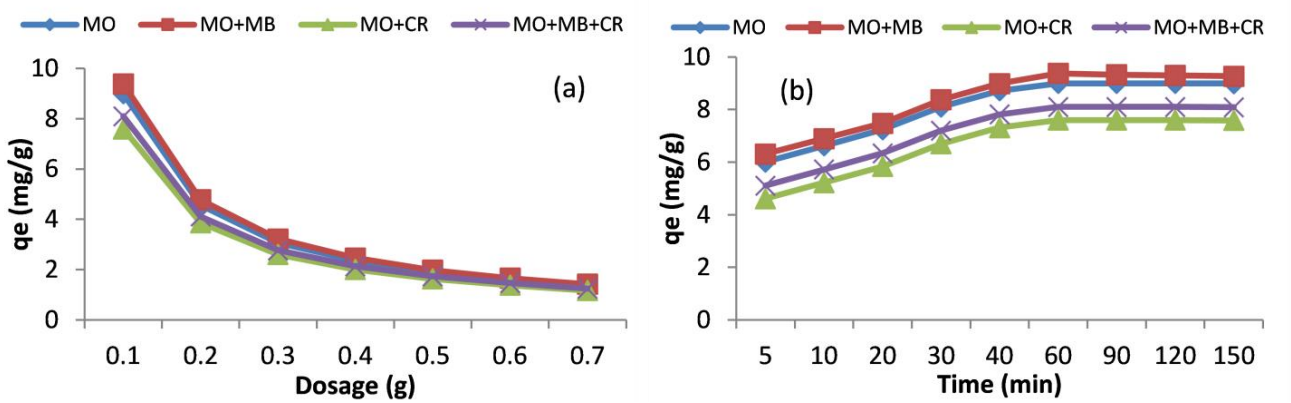

Figure 6: Effect of a) dosage, b) contact time.

3.4 Impact of Initial Concentration

To investigate how the initial concentration of methyl orange affects its absorption by the adsorbent, four different adsorbate systems were studied: (i) Methyl orange by itself (single system), (ii) Methyl orange combined with Methylene Blue (MO+MB, binary system), (iii) Methyl orange combined with Congo Red (MO+CR, binary system), and (iv) a mixture of methyl orange along with methylene blue and Congo red (MO + MB + CR, ternary system). The adsorbent's capacity for methyl orange, indicating the quantity of methyl orange adsorbed per unit mass of adsorbent, increased as the initial concentration of methyl orange increased in all types of adsorbate-adsorbent systems: single, binary, or ternary (Figure 6b).

As the initial concentration of methyl orange ranged from 20 – 500 mg/L, the values rose from 9.04 to 92.60 mg/g in the single system (MO), from 9.34 to 100.77 mg/g in the MO+MB binary system, from 7.64 to 57.60 mg/g in the MO+CR binary system, and from 8.54 to 80.10 mg/g in the ternary dye system. The observed increase in dye uptake with higher initial dye concentrations in all systems is likely due to the lower availability of dye molecules at lower concentrations. However, at higher concentrations, the abundance of dye molecules overcomes resistance to mass transfer.

Additionally, when starting with the same initial concentrations of methyl orange and other competing dyes, there were slight fluctuations in the adsorption capacity of all the systems. For example, at an initial concentration of 20 mg/L for methyl orange, the adsorption capacity of the adsorbent was 9.04, 9.34, 7.64, and 8.54 mg/g for the single, MO+MB, MO+CR, and MO+MB+CR systems, respectively. This behavior can be attributed to the competitive nature of the adsorption processes.

3.5 Influence of Contact Time and Kinetics

The adsorption of methyl orange exhibited a rise in the single, binary, and ternary dye systems as the contact time was extended, eventually reaching equilibrium (Figure 6b). This research delved into adsorption dynamics, which assesses the speed at which the solute is taken up, thereby influencing how long the adsorbate remains at the interface between solid and solution. The kinetics of methyl orange adsorption were explored using both the pseudo-first-order model and the pseudo-second-order equation. The mathematical expressions for these models are provided by equations 3 and 4 (28).

The pseudo-first-order equation:

$$\ln (q_e - q_t) = \ln q_e - k_1 t \quad (3)$$

The pseudo-second-order equation:

$$\frac{t}{q_t} = \frac{1}{k_2 q_e^2} + \frac{t}{q_e} \quad (4)$$

In this context, q_t (mg/g) represents the adsorption capacity at time t, k_1 (min^{-1}) stands for the rate constant of pseudo-first-order adsorption, and k_2 (g/mg/min) denotes the pseudo-second-order rate constant. Graphs depicting these equations can be found in Figure 7 (a and b), and the resulting rate parameters are listed in Table 2. Across all adsorbate systems (single, binary, and ternary), the adsorption kinetics were most accurately described by the pseudo-second-order rate model, with R^2 values exceeding 0.99. Additionally, both the experimental and calculated q_e values demonstrated better agreement with the pseudo-second-order model as opposed to the pseudo-first-order model. The conformity of sorption kinetics to the pseudo-second-

order equation implies that chemisorption likely plays a role in the rate-limiting step of the process (20).

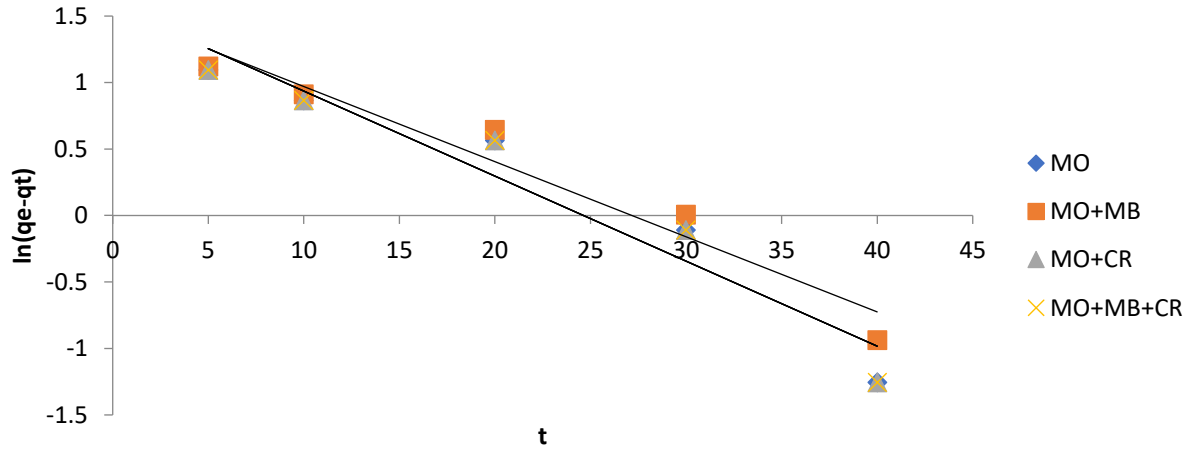

Figure 7: Pseudo-first order plot.

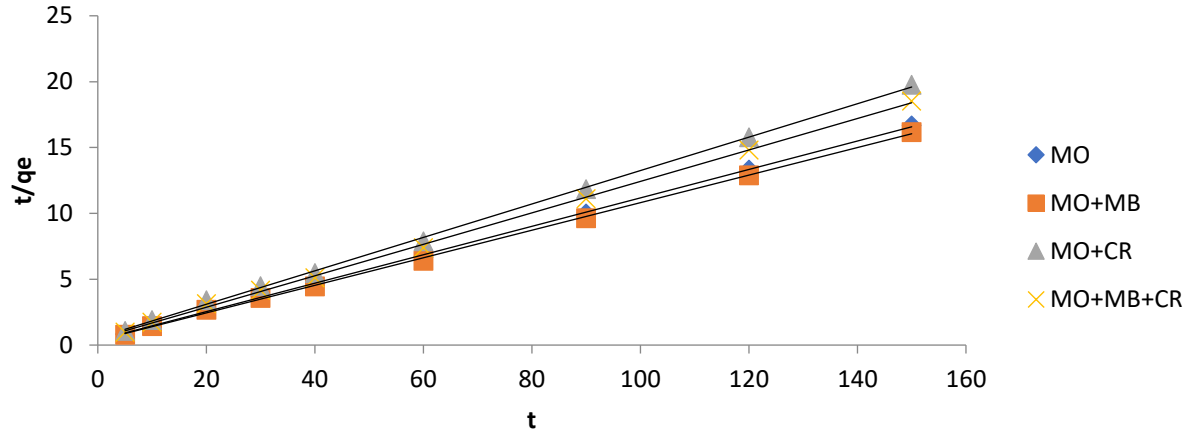

Figure 7b: Pseudo-second order plot.

Table 2: Kinetic parameters.

Kinetic Model	Parameters	MO	MO+MB	MO+CR	MB+MO+CR
Pseudo-first order	k_1	0.046	0.057	0.063	0.063
	$q_{e\ exp}$	9.00	9.38	7.60	8.10
	$q_{e\ cal}$	4.83	4.64	4.83	4.83
	R^2	0.9353	0.0.9459	0.9820	0.9353
Pseudo-second order	k_2	0.030	0.031	0.028	0.29
	$q_{e\ exp}$	9.00	9.38	7.60	8.10
	$q_{e\ cal}$	9.26	9.56	7.88	8.70
	R^2	0.9994	0.9993	0.9991	0.9999

3.6 Adsorption Isotherms

The adsorption equilibrium isotherm describes the connection between adsorbates in the liquid phase and those on the surface of the adsorbent under a consistent temperature. In this investigation, we employed linearized versions of the isotherm equations to fit the equilibrium concentrations of the remaining methyl orange dye solution (C_e) and the amounts of dye adsorbed onto the adsorbent surface (q_e) in single, binary, and ternary systems. This was carried out to characterize the equilibrium association under a constant temperature. The suitability of the isotherm models was evaluated based on the correlation coefficients (R^2) obtained from linear plots. The mathematical formulations utilized in this study are provided below:

Langmuir;

$$\frac{1}{q_e} = \frac{1}{q_{max} K_L C_e} + \frac{1}{q_{max}} \quad (5)$$

$$R_L = \frac{1}{1 + K_L C_0} \quad (6)$$

Freundlich;

$$\ln q_e = \ln K_f + \frac{1}{n} \ln C_e \quad (7)$$

Temkin $$q_e = b_T \ln C_e + b_T \ln K_T \quad (8)$$

where C_e stands for the equilibrium adsorbate concentration (mg/L), q_e represents the quantity of adsorbate absorbed per unit mass of adsorbent (mg/g), q_m and K_L are Langmuir constants associated with monolayer adsorption capacity and adsorbent affinity, respectively. R_L (L/mg) is a dimensionless Langmuir constant, and C_0 (mg/L) is the highest initial concentration. K_F is the Freundlich constant indicating adsorption capacity and intensity on the adsorbent or surface heterogeneity, while K_T and B_T are constants for the Temkin model. Additionally, R represents the universal gas constant (8.314 J mol·K), and T denotes the temperature in kelvin (29,30).

The equilibrium isotherm parameters and their corresponding correlation coefficients for the adsorption processes are provided in Table 3. The high values of the correlation coefficients (R^2) across the three isotherm models indicate distinct characteristics of the adsorption processes at different stages, thereby influencing the final mechanism. This suggests that the adsorption of methyl orange is a complex process.

Langmuir Isotherm Model: The Langmuir isotherm model posits that adsorption occurs as a monolayer on a finite number of surface sites without the adsorbate moving within the surface plane (31). For this study, the dimensionless (R_L) obtained for the entire system is less than 1, indicating favorable adsorption.

Freundlich Model: R^2 values for the adsorption processes were high, suggesting a potentially heterogeneous adsorbent surface and the likelihood of multilayer adsorption. The n values (Freundlich constant) above 1 for all adsorption processes indicate favorable adsorption (32).

Temkin Model: The Temkin isotherm was used to explore the energy relationship between adsorbate and adsorbent interactions. High R^2 values from the isotherm equation plots indicated model suitability. This suggests that the energy associated with methyl orange adsorption decreases linearly with coverage, in line with the Temkin model's assumption (33). This hints at adsorbate-adsorbate interactions in the studied adsorption processes.

The b_T constant, linked to adsorption energy, ranged from 1.99 to 3.92 kJ/mol. This range is lower than the 8–16 kJ/mol range associated with bonding energy in ion-exchange mechanisms. This implies that methyl orange and adsorbent interaction might involve physisorption rather than ion exchange. However, this doesn't rule out the possibility of chemisorption, as not all chemical interactions follow ion-exchange mechanisms. The alignment with the pseudo-second-order rate model suggests a role for chemisorption, particularly in the rate-determining step (34).

Table 3: Adsorption isotherm parameters.

Isotherm	Parameters	MO	MO+MB	MO+CR	MO+MB+CR
Langmuir	q_m (mg/g)	48.54	47.17	42.19	47.85
	K_L (L/mg)	0.11	0.18	0.05	0.07
	R_L	0.31	0.22	0.50	0.42
	R^2	0.9274	0.8979	0.9691	0.9491
Freundlich	K_F (mg/g)(L/mg)$^{1/n}$	6.83	7.94	4.32	3.23
	n	2.22	2.27	2.22	2.00
	1/n	0.45	0.44	0.45	0.0.50
	R^2	0.9935	0.9909	0.9886	0.9940
Temkin	A_T	16.35	16.77	11.70	15.15
	B_T	2.52	1.99	3.92	3.27
	R^2	0.8923	0.8698	0.9540	0.9170

3.7 Impact of Temperature and Thermodynamics

The influence of temperature on the adsorption process of Acid Blue 161 was investigated through batch adsorption experiments conducted at four distinct temperatures, 303 K, 313 K, 323 K, and 333 K, for both single and mixed systems. The outcomes are presented graphically in Figure 8. The figure clearly demonstrates that the adsorbent's adsorption capacity (q_e) for methyl orange dye decreases with increasing temperature in the single, binary, and ternary systems. This suggests that elevating the temperature reduces the adsorption of methyl orange dye, indicating that the adsorption process is more favorable at lower temperatures. Moreover, the rise in temperature likely induced changes in the morphology of the adsorbent, potentially causing destabilization of adsorbed adsorbate molecules (35).

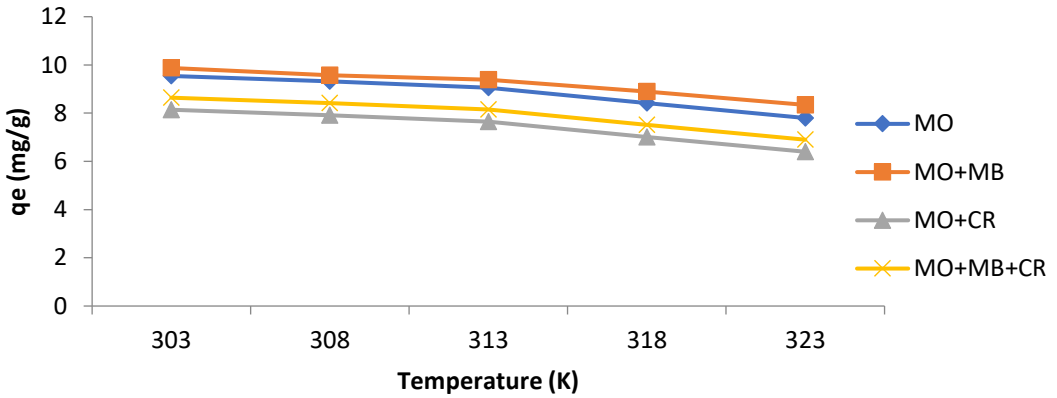

Figure 8: Effect of temperature.

The changes in free energy (ΔG), enthalpy (ΔH), and entropy (ΔS) were assessed as thermodynamic parameters from the batch adsorption results at different temperatures. The following equations were utilized:

$$K_c = \frac{C_{ads}}{C_e} \quad (9)$$

$$\Delta G = \Delta H - T\Delta S \quad (10)$$

$$ln\ K_c = \frac{\Delta S}{R} - \frac{\Delta H}{RT} \quad (11)$$

In these equations, K_c represents the sorption distribution coefficient, ΔG (kJ/mol) stands for the free energy of adsorption, T (Kelvin) denotes the absolute temperature, R is the universal gas constant, ΔH (kJ/mol) indicates the heat of adsorption, and ΔS (J/K) signifies the entropy change (36).

Figure 9 illustrates the ln K_c versus 1/T plots for methyl orange adsorption in both single and mixed systems at various temperatures. Enthalpy change (ΔH) and entropy change (ΔS) were determined from slopes and intercepts, while free energy changes (ΔG) were assessed using equation 9. All corresponding values are presented in Table 4.

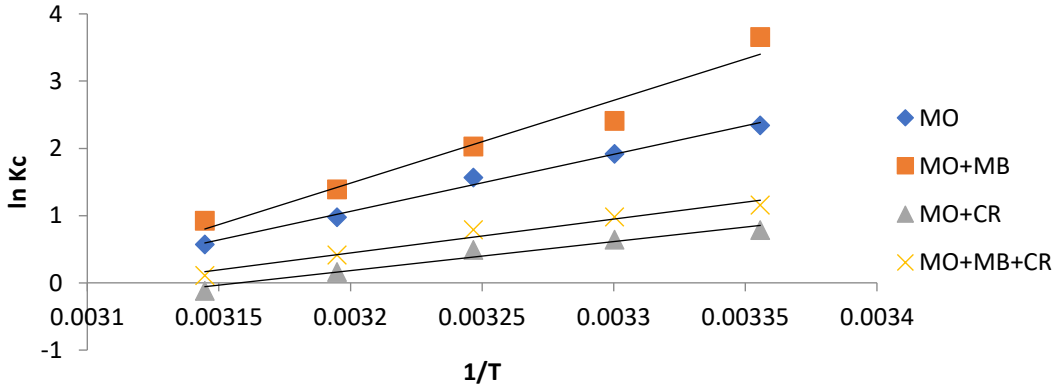

Figure 9: Thermodynamic plot.

Table 4: Thermodynamic parameters.

System	- ΔH (kJ/mol)	-ΔS (J/K)	-ΔG (kJ/mol)				
			303 K	308 K	313 K	318 K	323 K
MO	54.63	159.42	6.453	5.656	4.861	4.066	3.271
MO+MB	12.62	382.62	10.415	8.542	6.632	4.722	2.812
MO+CR	17.94	054.43	2.186	1.926	1.666	1.406	1.146
MO+MO+MB	22.58	064.55	3.190	2.870	2.550	2.230	1.910

The Gibbs free energy change (ΔG) for dye adsorption in all examined systems demonstrates a negative value, indicating spontaneous and thermodynamically feasible sorption processes (37). With decreasing temperatures, the feasibility of adsorption also increased in each system. Likewise, the adsorption processes in all systems were exothermic, as evidenced by their negative enthalpy values. This implies that heat was released during the interaction between the dye and the adsorbent surface. The entropy change (ΔS) exhibited negativities for all systems (Table 3). Negative ΔS

values suggest reduced randomness at the adsorbent and dye(s) interface in both single and mixture systems.

4. CONCLUSION

This investigation shows the effectiveness of gingerbread plum seed shell-activated carbon in removing methyl orange from aqueous solutions, encompassing single, binary, and ternary adsorbate systems. Various experimental parameters, including contact time, initial adsorbate concentration, adsorbent dosage, solution pH, and reaction temperature, were explored. The adsorption processes adhere to pseudo-second-order kinetics, while the Freundlich, Langmuir, and Temkin isotherm models exhibit high correlation coefficients (>0.9) in certain cases, indicating distinct characteristics at different stages that influence the final mechanism. All adsorption processes were confirmed to be spontaneous and thermodynamically viable, as evidenced by negative ΔG values. Additionally, they were exothermic in nature, leading to reduced randomness with negative ΔS values.

5. REFERENCES

1. Vatanpour V, Karimi H, Imanian Ghazanlou S, Mansourpanah Y, Ganjali MR, Badiei A, et al. Anti-fouling polyethersulfone nanofiltration membranes aided by amine-functionalized boron nitride nanosheets with improved separation performance. J Environ Chem Eng [Internet]. 2020 Dec 1;8(6):104454. Available from: <URL>.

2. Khan MA, Khan MI, Zafar S. Removal of different anionic dyes from aqueous solution by anion exchange membrane. Membr Water Treat [Internet]. 2017 May 25;8(3):259–77. Available from: <URL>.

3. Bhatia D, Sharma NR, Singh J, Kanwar RS. Biological methods for textile dye removal from wastewater: A review. Crit Rev Environ Sci Technol [Internet]. 2017 Oct 2;47(19):1836–76. Available from: <URL>.

4. Ragupathy S, Manikandan V, Devanesan S, Ahmed M, Ramamoorthy M, Priyadharsan A. Enhanced sun light driven photocatalytic activity of Co doped SnO2 loaded corn cob activated carbon for methylene blue dye degradation. Chemosphere [Internet]. 2022 May 1;295:133848. Available from: <URL>.

5. Bulgariu L, Escudero LB, Bello OS, Iqbal M, Nisar J, Adegoke KA, et al. The utilization of leaf-based adsorbents for dyes removal: A review. J Mol Liq [Internet]. 2019 Feb 15;276:728–47. Available from: <URL>.

6. George A, Magimai Antoni Raj D, Venci X, Dhayal Raj A, Albert Irudayaraj A, Josephine RL, et al. Photocatalytic effect of CuO nanoparticles flower-like 3D nanostructures under visible light irradiation with the degradation of methylene blue (MB) dye for environmental application. Environ Res [Internet]. 2022 Jan 1;203:111880. Available from: <URL>.

7. Noreen S, Bhatti HN, Nausheen S, Sadaf S, Ashfaq M. Batch and fixed bed adsorption study for the removal of Drimarine Black CL-B dye from aqueous solution using a lignocellulosic waste: A cost affective adsorbent. Ind Crops Prod [Internet]. 2013 Oct 1;50:568–79. Available from: <URL>.

8. Nausheen S, Bhatti HN, Sadaf S, Farrukh Z, Noreen S. Equilibrium Modeling of Removal of Drimarine Yellow HF-3GL Dye from Aqueous Solutions by Low Cost Agricultural Waste. J Chem Soc Pakistan [Internet]. 2014;36(1):177–90. Available from: <URL>.

9. Sadaf S, Bhatti HN, Nausheen S, Noreen S. Potential Use of Low-Cost Lignocellulosic Waste for the Removal of Direct Violet 51 from Aqueous Solution: Equilibrium and Breakthrough Studies. Arch Environ Contam Toxicol [Internet]. 2014 May 28;66(4):557–71. Available from: <URL>.

10. Das P, Debnath A. Reactive orange 12 dye adsorption onto magnetically separable CaFe2O4 nanoparticles synthesized by simple chemical route: kinetic, isotherm and neural network modeling. Water Pract Technol [Internet]. 2021 Oct 1;16(4):1141–58. Available from: <URL>.

11. Das P, Debnath P, Debnath A. Enhanced sono-assisted adsorptive uptake of malachite green dye onto magnesium ferrite nanoparticles: Kinetic, isotherm and cost analysis. Environ Nanotechnology, Monit Manag [Internet]. 2021 Dec 1;16:100506. Available from: <URL>.

12. Das P, Nisa S, Debnath A, Saha B. Enhanced adsorptive removal of toxic anionic dye by novel magnetic polymeric nanocomposite: optimization of process parameters. J Dispers Sci Technol [Internet]. 2022 May 2;43(6):880–95. Available from: <URL>.

13. Deb A, Debnath A, Saha B. Sono-assisted enhanced adsorption of eriochrome Black-T dye onto a novel polymeric nanocomposite: kinetic, isotherm, and response surface methodology optimization. J Dispers Sci Technol [Internet]. 2021 Aug 31;42(11):1579–92. Available from: <URL>.

14. Olajire AA, Giwa AA, Bello IA. Competitive adsorption of dye species from aqueous solution onto melon husk in single and ternary dye systems. Int J Environ Sci Technol [Internet]. 2015 Mar 9;12(3):939–50. Available from: <URL>.

15. Giwa AA, Oladipo MA, Abdulsalam KA. Adsorption of Rhodamine B from single, binary and ternary dye systems using sawdust of Parkia biglobosa as adsorbent: isotherm, kinetics and thermodynamics studies. J Chem Pharm Res [Internet]. 2015;7(2):454–75. Available from: <URL>.

16. Husaini M, Usman B, Ibrahim MB. Adsorption Studies of Methylene Blue using Activated Carbon Derived from Sweet Detar Seed Shell. ChemSearch J [Internet]. 2023 Jul 27;14(1):21–32. Available from: <URL>.

17. Ibrahim MB, Umar A. Adsorption thermodynamics of some basic dyes uptake from aqueous solution using Albizia lebbeck shells. ChemSearch J [Internet]. 2016 Jul 27;7(1):43–51. Available from: <URL>.

18. Moharm AE, El Naeem GA, Soliman HMA, Abd-Elhamid AI, El-Bardan AA, Kassem TS, et al. Fabrication and Characterization of Effective Biochar Biosorbent Derived from Agricultural Waste to Remove Cationic Dyes from Wastewater. Polymers (Basel) [Internet]. 2022 Jun 26;14(13):2587. Available from: <URL>.

19. Husaini M, Bashir Ibrahim M. Investigation of Inhibition Potential Effect of Organic Compound for the Corrosivity of Phosphoric Acid on Aluminium. Int J Eng Manuf [Internet]. 2020 Feb 8;10(1):41–53. Available from: <URL>.

20. Husaini M, Bashir Ibrahim M. Thermodyamic and Kietic Study on the Corrosion of Aluminium in Hydrochloric Acid

using Benzaldehyde as Corrosion Inhibitor. Int J Eng Manuf [Internet]. 2019 Nov 8;9(6):53–64. Available from: <URL>.

21. Ekpete OA, Horsfall MJ. Preparation and Characterization of Activated Carbon derived from Fluted Pumpkin Stem Waste (Telfairia occidentalis Hook F). Res J Chem Sci. 2011;1(3):10–7.

22. Ibrahim MB. Comparative analysis of the thermodynamics and adsorption isotherms for the adsorption of some metal ions from aqueous solution using sawdust material. Int J Res Chem Environ [Internet]. 2011;1(1):179–85. Available from: <URL>.

23. Saranya KS, Vellora Thekkae Padil V, Senan C, Pilankatta R, Saranya K, George B, et al. Green Synthesis of High Temperature Stable Anatase Titanium Dioxide Nanoparticles Using Gum Kondagogu: Characterization and Solar Driven Photocatalytic Degradation of Organic Dye. Nanomaterials [Internet]. 2018 Dec 4;8(12):1002. Available from: <URL>.

24. Kim JR, Kan E. Heterogeneous photo-Fenton oxidation of methylene blue using CdS-carbon nanotube/TiO 2 under visible light. J Ind Eng Chem [Internet]. 2015 Jan 25;21:644–52. Available from: <URL>.

25. Husaini M, Usman B, Ibrahim MB. Competitive Adsorption of Congo red Dye from Aqueous Solution onto Activated Carbon Derived from Black Plum Seed Shell in Single and Multicomponent System. African J Manag Eng Technol Cit [Internet]. 2023;2023(2):76–89. Available from: <URL>.

26. Giwa ARA, Abdulsalam KA, Wewers F, Oladipo MA. Biosorption of Acid Dye in Single and Multidye Systems onto Sawdust of Locust Bean (Parkia biglobosa) Tree. J Chem [Internet]. 2016;2016:6436039. Available from: <URL>.

27. Husaini M, Usman B, Ibrahim MB. Modeling and Equilibrium Studies for the Adsorption of Congo red Using Detarium microcarpum Seed Shell Activated Carbon | Applied Journal of Environmental Engineering Science. Appl J Environ Eng Sci [Internet]. 2023 [cited 2024 Feb 28];9(3):147–62. Available from: <URL>.

28. Ho Y. Review of second-order models for adsorption systems. J Hazard Mater [Internet]. 2006 Aug 25;136(3):681–9. Available from: <URL>.

29. Langmuir I. The adsorption of gases on plane surfaces of glass, mica and platinum. J Am Chem Soc [Internet]. 1918 Sep 1;40(9):1361–403. Available from: <URL>.

30. Freundlich H. Über die Adsorption in Lösungen. Zeitschrift für Phys Chemie [Internet]. 1907 Oct 1;57U(1):385–470. Available from: <URL>.

31. Temkin MI. Kinetics of ammonia synthesis on promoted iron catalysts. Acta Physiochim [Internet]. 1940;12:327–56. Available from: <URL>.

32. Sekar M, Sakthi V, Rengaraj S. Kinetics and equilibrium adsorption study of lead(II) onto activated carbon prepared from coconut shell. J Colloid Interface Sci [Internet]. 2004 Nov 15;279(2):307–13. Available from: <URL>.

33. Juang LC, Wang CC, Lee CK, Hsu TC. Dyes adsorption onto organoclay and MCM-41. J Environ Eng Manag [Internet]. 2007;17(1):29–38. Available from: <URL>.

34. Giwa A, Olajire A, Adeoye D, Ajibola T. Kinetics and Thermodynamics of Ternary Dye System Adsorption on to Melon (Citrillus lanatus) Seed Husk. Am Chem Sci J [Internet]. 2015 Jan 10;7(1):7–25. Available from: <URL>.

35. Tian W, Lin J, Zhang H, Duan X, Wang H, Sun H, et al. Kinetics and mechanism of synergistic adsorption and persulfate activation by N-doped porous carbon for antibiotics removals in single and binary solutions. J Hazard Mater [Internet]. 2022 Feb 5;423:127083. Available from: <URL>.

36. Husaini M, Usman B, Ibrahim MB. Inhibitive Effect of Glutaraldehyde on the Corrosion of Aluminum in Hydrochloric Acid Solution. J Sci Technol [Internet]. 2019 Dec 30;11(2):8–16. Available from: <URL>.

37. Husaini M, Usman B, Ibrahim MA, Ibrahim MB. Effect of Aniline as Corrosion inhibitor on the Corrosion of Aluminium in Hydrochloric Acid Solution. Res J Chem Environ. 2020;24(2):99–106.